Studies on mechanical properties of Al base nanocomposite

S.Hembrom[a], B.N.Roy[a], D.Roy[b]
[a]*Department of Metallurgical Engineering, BIT, Sindri, Dhanbad-828123*

[b]*Department of Materials and Metallurgical Engineering, NIFFT, Ranchi-834003*

Abstract— Mechanically alloyed Al50Ti40Si10 nanocrystalline alloy powder was consolidated by Hot isostatic pressing in the range 300-600oC with a pressure of 1.2 GPa. Phase and microstructural evolution at appropriate stages of mechanical alloying/blending and sintered compact was monitored by X-ray diffraction and scanning and transmission electron microscopy. Alloy sintered at 500oC recorded an excellent combination of high hardness (8.61 GPa) compressive strength (1212 MPa), shear strength (600 MPa) and Young's modulus (149 GPa).

Index terms- Aluminum alloy; Mechanical Alloying; Hot isostatic pressing; Composite

1 INTRODUCTION

High strength to weight ratio is an essential criterion for design and selection of a material for structural applications in transportation and aviation industries. In this connection, Al-alloys are the most widely used materials. It is known that the maximum tensile strength level of age hardenable Al-alloys are limited to about of 500-600 MPa. In contrast, compressive strength of Al-alloys can be increased to as high as 1200-1400 MPa in amorphous or nanocrystal dispersed amorphous condition [1-3]. Among various techniques, mechanical alloying has emerged as a versatile solid-state synthesis route to develop amorphous alloys with metastable microstructure [4-6]. Furthermore subsequent heat treatment of the mechanical alloyed amorphous matrix product may enable dispersion of nanocrystalline intermetallic phases [7-8]. Hot/warm pressing or extrusion is a possible method to fabricate bulk sample from mechanically alloyed amorphous powders [9-10]. Sintering at high pressure and temperature for prolonged period proves counter productive, as it leads to partial crystallization of the amorphous phase, or grain coarsening of the nanocrystalline aggregate [11-13]. Therefore, consolidation of mechanically alloyed amorphous/nanocrystalline powders into fully dense bulk structure presents a major challenge towards developing high specific strength Al-alloys with amorphous, nanocrystalline or nano-intermetallic dispersed amorphous microstructure. It is known that mechanical properties of nanocrystalline materials are highly sensitive to the presence of internal defects, heterogeneities and grain size distributions, caused during the consolidation of the nanocrystalline powders [14-16]. Hence, the consolidation process needs to be optimized for production of dense nanocrystalline materials with narrow grain size distributions.

In the recent years, the hot isostatic pressing (HIP) has emerged as a versatile technique to obtain dense and near-net shape bulk product from nanometer-size powders [17-18]. Hot isostatic pressing involves the simultaneous application of an elevated temperature and a high-pressure (usually inert) gas in a specially constructed vessel or container [19]. The applied pressure is isostatic because it is developed with a gas, so that, at least as a first approximation, no alteration in component geometry occurs. Under suitable conditions of heat and pressure, internal pores or defects within a solid body collapse and weld up to obtain high density compacts without large scale change in the component shaped or dimension[20]. The processing time is shorter compared to conventional sintering which prevents excessive grain growth, thereby yielding relatively high yield strength and toughness associated with finer grain sizes in the products [21]. Densification of compacts depends on many processing parameters such as temperature, pressure, and material parameters such as powder size, creep and diffusion constants.

The mechanical behavior of nanocrystalline metals is a research topic of considerable interest for the past two decades. The shear-punch test is an efficient technique for evaluating mechanical properties, particularly when material availability or component size is limited. The mechanical properties, such as yield and ultimate strengths, as well as strain hardening exponent values can be calculated from the shear punch test data [22]. A linear correlation between the shear punch test and tensile data has been reported earlier by many investigators [23-24]. Though this technique was initially employed for testing of conventional metals and alloys, it has been subsequently been extended to heterogeneous materials like composites and multi-phase aggregates [25]. The procedure for shear punch test is similar to the blanking operation, where a flat solid punch is used to shear a sheet material through a die at a constant rate. The stress-strain curve obtained from this test based on shearing operation has many similarities to tensile test response as both comprises an initial linear elastic region, the yield point, a region representing plastic deformation and an ultimate (maximum) load. As quantity and dimension / size of bulk amorphous or nanocrystalline material or component is often restricted and too small to conduct tensile studies, shear punch test can be convenient and ideal technique to estimate approximately the tensile strengths of nano crystalline materials [26].

In the present work, mechanically alloyed $Al_{50}Ti_{40}Si_{10}$ amorphous/nanocrystalline powders have been sintered by hot isostaic pressing to obtain nano-intermetallic dispersed amorphous matrix composite microstructure. The microstructures have been investigated by X-ray diffraction and trans-

mission electron microscope. Furthermore, mechanical properties such as hardness, Young's modulus, shear strength, compressive strength and compressive fracture mechanism of the composites have been investigated.

2 EXPERIMENTAL PROCEDURE

Appropriate amounts of Al–Ti–Si elemental powders (with each constituent having at least 99.5 wt% purity and about 50–100 μm particle size) in the nominal stoichiometry of $Al_{50}Ti_{40}Si_{10}$ were subjected to mechanical alloying in a Retsch PM 400 high-energy planetary ball mill operated at 300 rpm with 10:1 ball to powder weight ratio using tungsten carbide (WC) coated vial and balls (10 mm diameter). Milling was carried out in wet (toluene) medium to avoid agglomeration, retard oxidation, and prevents coating of milling media (balls and vial) with Al. Fully amorphous $Al_{50}Ti_{40}Si_{10}$ alloy was obtained after 10 h of mechanical milling.

Thereafter, the mechanically alloyed powder was sealed into a steel can or cylinder in vacuum, and was processed in ultra-high pressure HIP equipment in order to consolidate the powders. The powder volume was heated in temperature range 300-600^{o}C under an isostatic pressure of 1.2 GPa in Ar gas for about 10 min. Studies on the microstructural evolution, mechanism of solid state amorphisation and thermal stability of the $Al_{50}Ti_{40}Si_{10}$ amorphous alloy has already been reported elsewhere [27]. Identity and volume fraction of phases in sintered samples were determined by high resolution X-ray diffraction (XRD) using a Panalytical X'Pert Pro diffractometer with Cu *Ka* (0.1542 nm) radiation. Microstructure and micro-composition of different phases of the composite samples were investigated using field emission gun assisted scanning electron microscope (FESEM, Carl Zeiss, Supra 40) and high resolution transmission electron microscope (HRTEM, JEOL 2100) with energy dispersion spectroscopy (EDS).

The average hardness and modulus of elasticity of the composite samples was measured with the help of a nano indentation tester (Nanoindentor-XP, Nanoinstrument incorporate, USA) at 500 mN load averaged from 15-20 indentations at equivalent locations on the same sample (within a standard deviation with 1%). Density of the compacted and sintered samples was measured using a helium pycnometer (AccuPyc1330).

Compression tests were carried out at a strain rate of 1x $10^{-3}s^{-1}$ at room temperature using a universal testing machine. The load and displacement were measured by using a quartz load cell of 5 kN capacity (accuracy ± 1 N) and high accuracy digital strain gauge (accuracy ± 1μm), respectively. During compression test, deformation and micro-cracking in the sample were monitored through acoustic emission signals using acoustic emission measuring system. The apparatus for such measurement was presented elsewhere [28]. The fracture surfaces of the composite after compression test were studied using an FESEM.

Shear punch tests were carried out on 250 – 400 μm thick samples. The die and punch used for shear punch test were procured from Pivot – Punch Corporation, New York, USA. A schematic illustration of the test geometry indicating the idealized pure shear deformation zone is shown in Fig. 1 The specific dimensions used for the test: diameter of the punch (d_{punch}) = 0.982 mm, diameter of the die (d_{die}) = 1 mm and clearance (c) = (d_{die} - d_{punch})/2 = 9 μm. These parameters were chosen to maximize the shear loading for a high strength material. The punch was connected to a load cell with a capacity of 10 kN. Disk samples cut from the sintered composite were ground flat with 600, 1200, 2400 and 4000 grit polishing papers. Final polishing to obtain mirror surface was done on clothes by using 0.1 μm alumina powder slurry. Load (L) versus punch displacement (Δ) curves were obtained at a punch displacement speed of 0.24 mm/s. Shear failure mechanism investigated by observation of fracture surface using an FESEM. The average shear stress (τ) was computed from the empirical relation: $\tau = L / (\pi d_{mean} h)$, where d_{mean} is the mean of the punch and die diameters and h is the specimen thickness. The shear stress computed in this manner has been shown to correlate well with uniaxial tensile test results for polycrystalline metal and alloys [29]. For pure shear, the associated strain is normally given by $\gamma = \Delta/c$. However, this relation is generally not used for shear punch test because the strain involved during the test is spatially distributed outward from an idealized zone as shown in Fig. 1 [30]. It is generally assumed that the average shear strain and strain rate are proportional to the punch displacement and punch speed, respec-

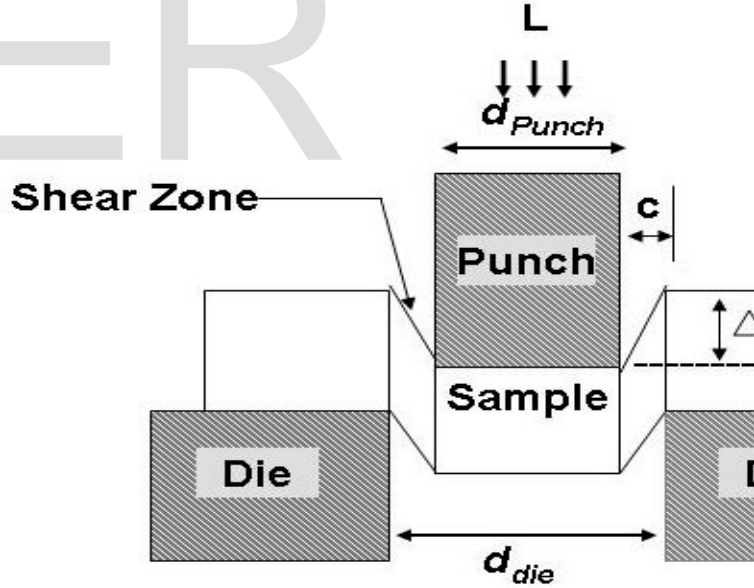

Fig.1 Schematic of shear punch test set up

3 RESULTS AND DISCUSSION

Fig. 2 shows the XRD patterns from the $Al_{50}Ti_{40}Si_{10}$ elemental powder blend subjected to mechanical alloying in planetary ball mill for 1, 10 and 15 h, respectively. It is evident that the characteristic peaks of the constituent elements in Fig. 2(b) disappear after 10 h of mechanical milling. However, a low

intensity and broad peak of Al_3Ti is found superimposed on the broad hump representing the amorphous matrix. This phase aggregate corroborates the results of a previous study dealing with mechanical alloying of the same powder blend [31-32]. Fig. 3 shows the high resolution TEM image and corresponding SAD pattern from the $Al_{50}Ti_{40}Si_{10}$ blend following mechanical alloying in a planetary mill for 10 h. It is evident that the microstructure is predominantly amorphous with isolated nanocrystalline regions confined to less than 8 nm. The presence of a diffuse halo and a faint ring in the SAD pattern representing Al_3Ti indicate that the milled product at this stage contains amorphous and nanocrystalline areas. Thus Fig 3 corroborates the XRD results in Fig. 2 and confirms that the microstructure consists of a mixture of an amorphous and nanocrystalline Al_3Ti phase.

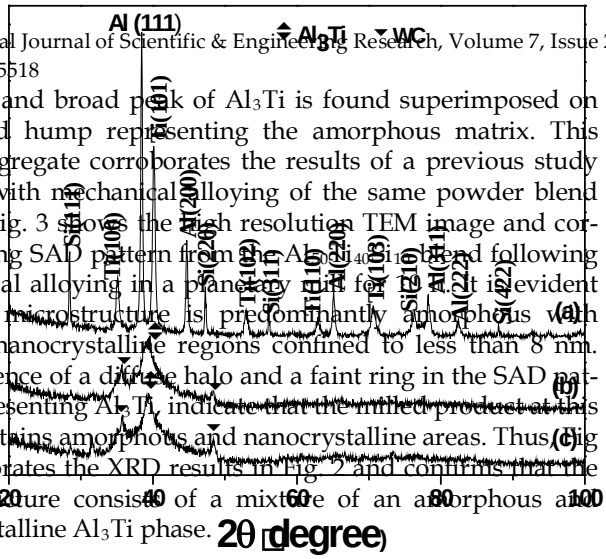

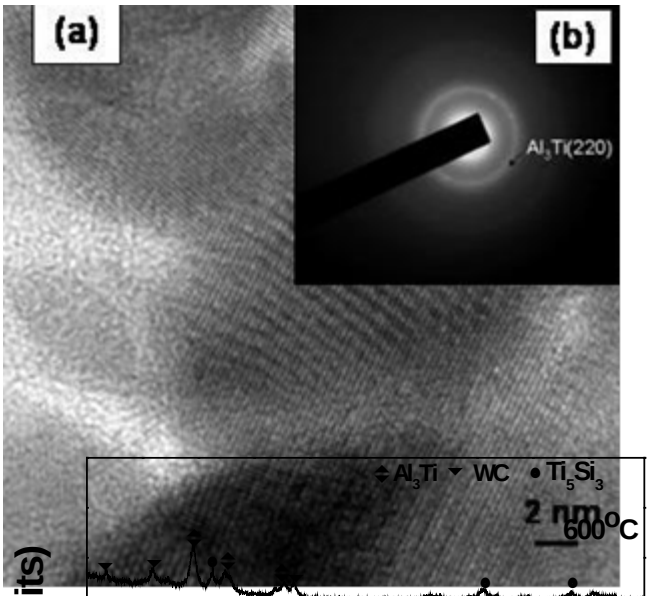

Fig. 3 TEM image of the $Al_{50}Ti_{40}Si_{10}$ alloy following mechanical alloying for 10 h (a) High resolution image and (b) the corresponding SAD pattern

Fig. 4 shows the XRD patterns of the composite after hot isostatic pressing in the temperature range 300-600°C. The patterns suggest that sintering has led to crystallization of the as-milled partially amorphous aggregate into dispersion of several ultrafine intermetallic phases like Al_3Ti and Ti_5Si_3 in varying volume fraction in the remnant amorphous matrix. Peaks of these phases seem superimposed on the halo of the as-milled product suggesting that sintering produces a metastable composite microstructure containing several intermetallic phases dispersed in amorphous matrix.

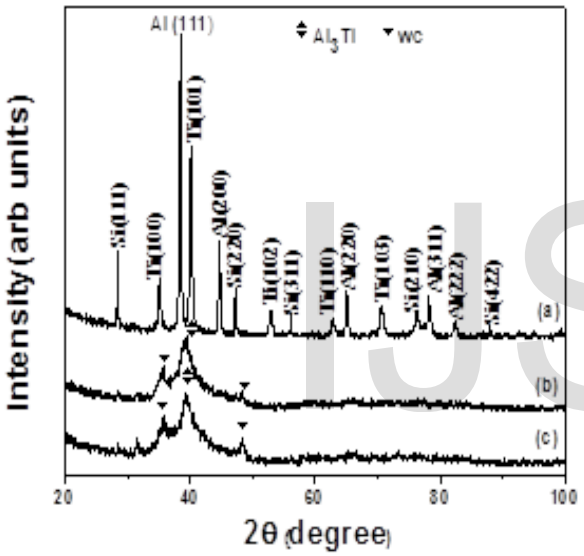

Fig.2 XRD patterns from the $Al_{50}Ti_{40}Si_{10}$ elemental powder blends obtained by mechanical alloying for (a) 1 h, (b) 5 h and (c) 10 h

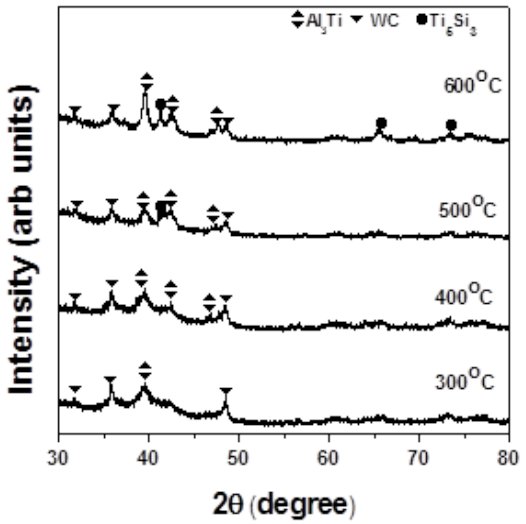

Fig.4 XRD patterns of the $Al_{50}Ti_{40}Si_{10}$ amorphous matrix composite consolidated by hot isostatic pressing at different tem-

perature.

Bright field TEM image and corresponding SAD pattern from the composite consolidated at 500°C are shown in Figs. 5a and 4b, respectively. Examination of the TEM image (Fig. 5a) and indexing of the Debye rings in the SAD pattern (Fig. 5b) indicate that nanometric (≈50 nm) precipitates of Al_3Ti, and Ti_5Si_3 are dispersed in the Al-rich partially amorphous matrix of the composite consolidated at 500°C. Thus Fig.5 corroborates the results obtained by XRD analysis in Fig. 4.

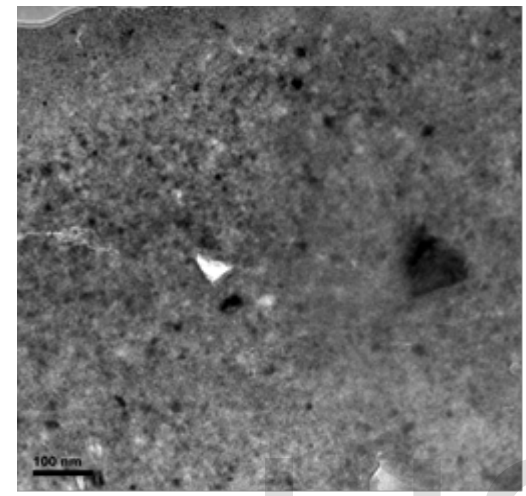

(a)

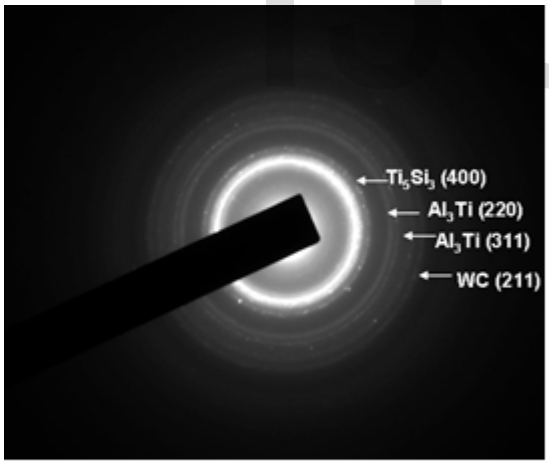

(b)

Fig.5 Composite consolidated by hot isostatic pressing at 500°C: (a) Bright field TEM image, and (b) the corresponding SAD pattern.

Fig. 6a shows typical bright field TEM images of the composite consolidated at 600°C, while a selected area diffraction pattern from same microstructure is presented in Fig. 6b. Comparison of the TEM images in Figs. 5a and 6a indicate that the volume fraction of crystalline phases is greater in the latter. In fact, the SAD pattern from the composite sintered at 600°C (Fig. 6b) clearly shows sharp Debye rings, without the diffuse halo contributed by the amorphous region. In other words, the rings of the SAD pattern in Fig. 6b represent a predominantly nanocrystalline structure. As expected, the present TEM investigation has revealed that the amorphous-nanocrystalline phase transformation is promoted to a larger extent at the higher temperature.

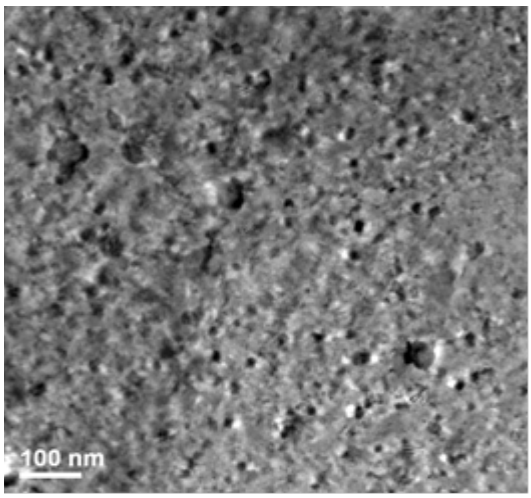

(a)

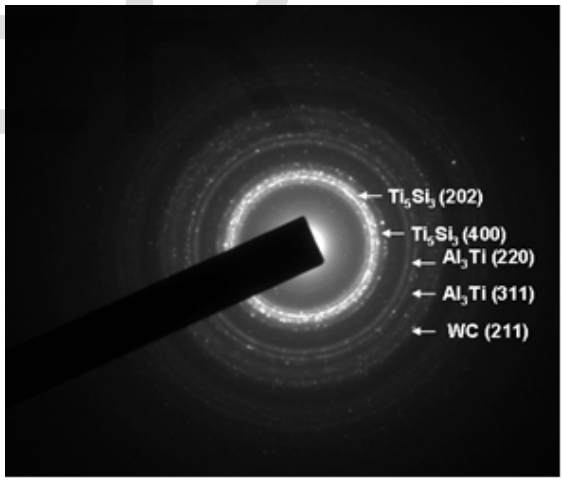

(b)

Fig.6 Composite consolidated by hot isostatic pressing at 600°C: (a) Bright field TEM image, and (b) the corresponding SAD pattern

Fig. 7shows the variation of density of the sintered compacts with temperature of consolidation. It is apparent that the maximum density is observed in the composite sintered at 600°C, and lowest density is exhibited by the composite consolidated at 400°C temperature. While the lowest density on compacting at 400°C temperature is due to incomplete grain-bridge formation or cold welding and presence of porosities, greater density at 500-600°C is facilitated by greater de-

gree/extent of diffusion at higher temperatures for identical time period. It may be noted that the difference in density or porosity levels in the products obtained by sintering at 500 and 600°C is marginal.

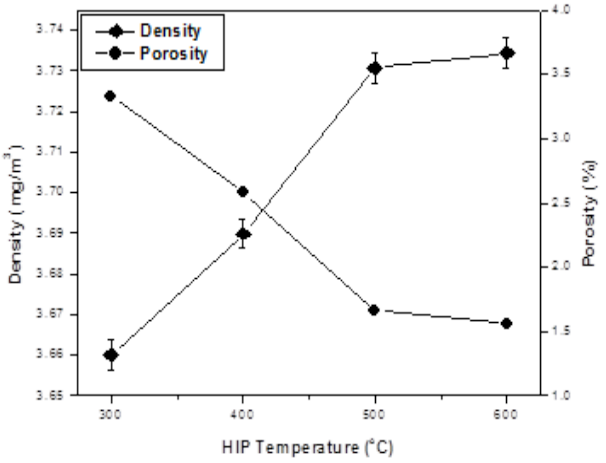

Fig.7 Plots depicting the variation Variation of density and porosity of the composite as a function of the temperature for hot isostatic pressing

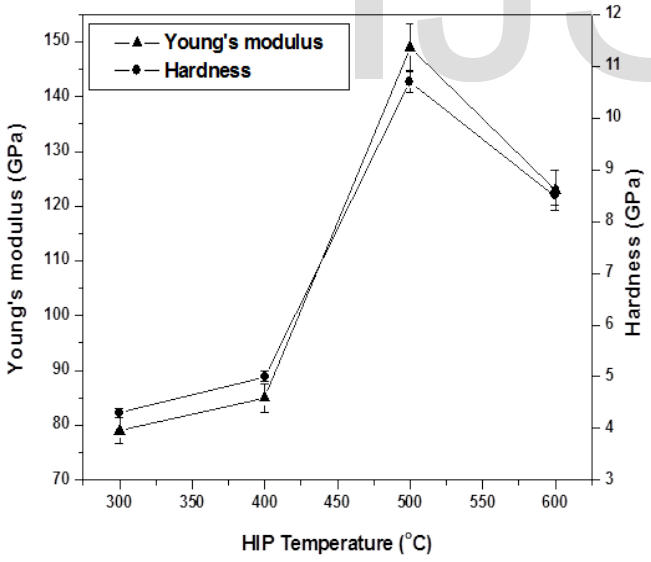

Fig. 8 Plots presenting the young's modulus and hardness of the composite as a function of the temperature used for HIP during consolidation.

Fig. 8 shows the variation of the Young's modulus and hardness of the mechanically alloyed and sintered $Al_{50}Ti_{40}Si_{10}$ powder samples as a function of the temperature of hot isostatic pressing. It is apparent that pressing at 500°C yields the composite with the highest hardness and Young's modulus. Based on the observations from Fig.8 it is possible to infer that the maximum Young's modulus and hardness is obtained after pressing at 500°C. It is interesting to note that samples pressed at still higher temperature of 600°C have lower hardness and Young's modulus, than those pressed at 500°C. Both the decrease in hardness and Young's modulus on pressing at the higher temperature can probably be attributed to the transformation of amorphous matrix to nanocrystals as well as anomalous growth of the intermetallics precipitates taking place on a larger scale between 500° and 600°C. It has been previously reported that the Young's modulus of nanocrystalline metals and alloys is lower than that in the samples with coarse-grained structure, due to a large volume fraction of grain boundaries in the former [33,34]. The decrease in hardness may also be explained on the basis of activation of dislocations or deformation twinning during indentation in the fully crystalline samples, obtained by pressing at 600°C. Grain growth in isolated regions may also contribute to a significant decrease in hardness in localized areas.

Fig.9 shows the stress-displacement plots obtained during compression tests, carried out on the hot isostatic pressed composites at different temperatures. From the stress-displacement curves, it is obvious that failure has occurred in the elastic regime itself prior to yielding, indicating that compressive ductility is almost non-existent. The maximum compressive strength of 1212 MPa has been found in the composite pressed at 500°C. The process of fracture initiation and propagation has been monitored through the observation of the cumulative number of acoustic emission events recorded from the unit volume of the samples subjected to compressive loading (Fig. 10). In the plots of acoustic emission against stress, the stress corresponding to the initiation of failure is distinguished by the rapid increase of acoustic emission activity marked by the arrowheads in Fig. 10. From examination of the plots for the compact pressed at 500°C, it is apparent that the failure is initiated in the range of 1200 MPa.

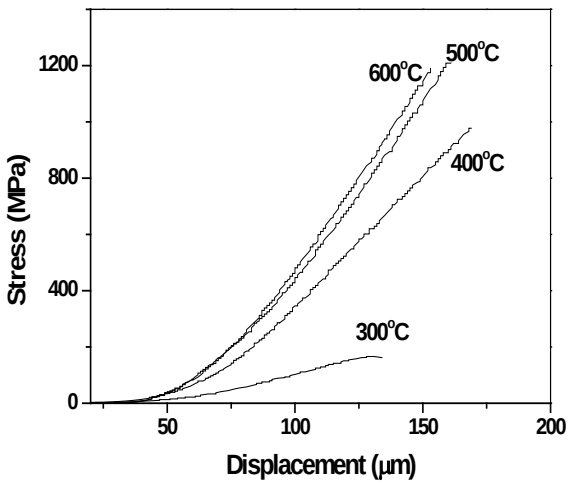

Fig.9 Variation of engineering stress with displacement for the composite prepared by hot isostatic pressing at different temperature

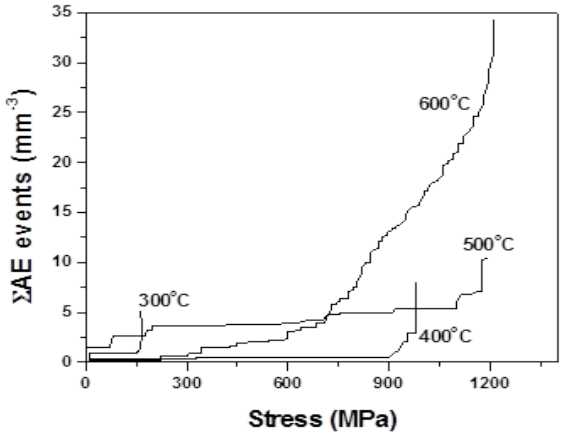

Fig.10 Variation of cumulative acoustic emission events against the compressive stress recorded during deformation of the compacts sintered by hot isostatic pressing at different temperature.

The fracture surfaces formed due to compression tests are shown in Fig. 11(a) and (b). Examination of the SEM images of the fracture surfaces records evidence of primarily brittle failure, which is obvious from the corresponding stress - displacement plots in Fig. 9. Fig. 10 (a) shows evidence of secondary cracking and shear accompanying deformation prior to failure. The presence of secondary cracks is consistent with the presence of multiple acoustic emission events near the fracture stress. The roughness of the fracture surface is attributed to deformation by microscopic and localized shear, although the macroscopic plastic strain is non-existent (Fig. 9). On the other hand, examination of the SEM fractograph in Fig. 11(b) shows presence of nano-size particles exposed on the fracture surface, suggesting that failure involves interfacial decohesion of individual or clusters of nanocrystalline Al_3Ti particles with spheroidal shapes from the amorphous Al-Ti-Si alloy matrix. It is suggested that ductility of the composite could be improved by inhibiting the separation of the nanometric particles, and promoting the shear.

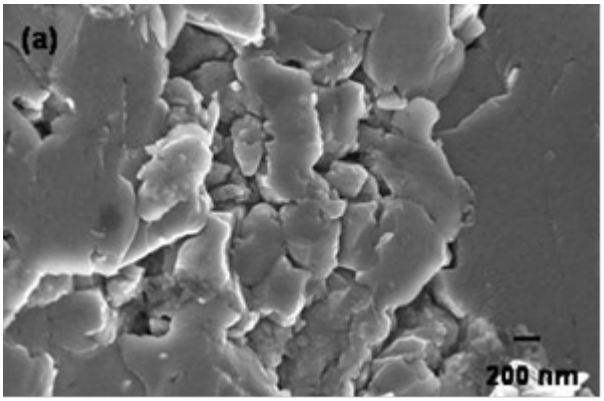

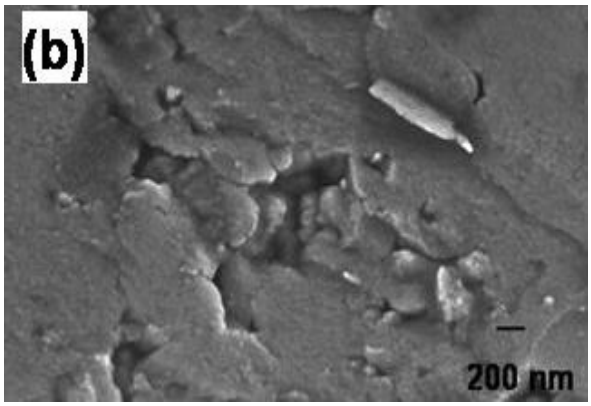

Fig.11 FESEM images of the fracture surfaces generated during compression tests carried out with the compacts consolidated by hot isostatic pressing at: (a) 500°C (b) 600°C.

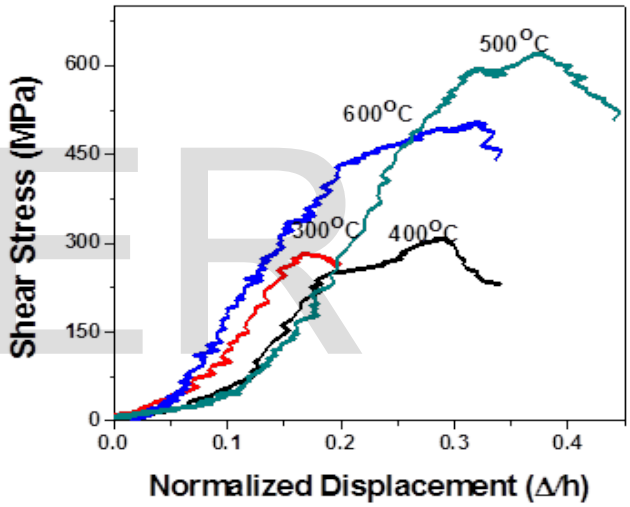

Fig.12 Plots showing the variation of shear stress with normalized displacement for the composite samples prepared by hot isostatic pressing at different temperature

Fig. 12 records the variation of shear stress (τ) with normalized displacement (Δ/h) recorded during shear punch test (as per the scheme shown in Fig.1) for the composites processed at different temperatures. These curves show an initial rise in stress with displacement until the ultimate shear stress is reached, followed by a drop in stress due to disk separation and punch through. The initial increase in stress with displacement is almost linear, as is expected for predominantly elastic deformation. The ultimate shear stress τ_u is defined as the maximum stress reached in the τ versus Δ/h curve. To predict the ultimate tensile strength values from the shear punch test data, the empirical relationship proposed by Guduru et al. [30] was used:

$$\sigma_{UTS} = 1.8\ \tau_{UTS} \quad (2)$$

where τ_{UTS} = ultimate shear strength and σ_{UTS} = ultimate ten-

sile strength.

The results in Fig. 12 indicate that the drop in stress occurs sharply after the σ_{UTS} is reached, while evidence of yielding is apparent in the curves representing the composite sintered at temperature of 400°C. The ultimate stress is found to exceed the apparent limit (deviation from linearity), and this phenomenon observed earlier for uniaxial compression tests has been attributed by researchers to a rise in the plastic flow resistance similar to strain hardening [35, 36]. Koch et al [37] reported that the elastic limit for the τ versus Δ/h curves does not correspond to a physically meaningful yield point. Due to the gradual development of general plasticity in the deformation zone (Fig. 1), along with punch die-sample compliance effects that can be non-linear, a 1% plastic offset in Δ/h is needed to reach the shear yield point for typical polycrystalline metals [30]. Owing to a more extensive elastic-plastic transition and lack of strain hardening capability in amorphous material, the yield point offset is expected to be significantly larger. This phenomenon requires further systematic investigation. The present study focused attention on the ultimate shear stress at failure, τ_u, with an attempt to determine its relationship with uniaxial compressive test results.The average ultimate shear stress values for the composites sintered at 500°C and 600°C are 600 ±10 MPa and 500 ± 10 MPa respectively, while their failure stress, σ_c , in uniaxial compression tests are 1200 ± 10 MPa and 1150 ± 10, respectively. Liu et al. [38] reported that pressure independent ultimate shear stress, τ_u, is related to compression data by the following expression:

$$\tau_u = \sigma_c \sin^2\theta, \quad \text{(i)}$$

where θ is shear plane angle. The value of τ_u estimated theoretically by substituting the experimentally determined values of σ_c in relation (2) is found mechanical property data obtained by shear punch test comparable to the composite sintered at 500 and 600°C (600 MPa and 500 MPa).Thus, the results of this study conclusively indicates that the shear punch test could be reasonably used to measure the pressure independent shear stress of nano-composites.

4 CONCLUSION

Composites with partially amorphous matrix were synthesized by mechanical alloying of $Al_{50}Ti_{40}Si_{10}$ elemental powder blend in high energy planetary ball mill followed by hot isostatic pressing. The microstructure of composites sintered at range of 300-600°C showed nano-size (≈50 nm) crystalline precipitates dispersed in amorphous matrix.

The major conclusions that emerged out of the present study are:

1. Hot isostatic pressing is a possible way for consolidation of mechanically alloyed powders into bulk nanocomposite. The sintered component records homogeneous microstructure with high density without defect or cracks
2. XRD analysis shows that mechanical alloying gives rise to amorphous/nanocrystalline microstructure after 10 h of milling. TEM micrographs also substantiate the XRD results.
3. The $Al_{50}Ti_{40}Si_{10}$ composite shows optimum values of hardness (8.61 GPa) compressive strength (1212 MPa), shear strength (600MPa) and Young's modulus (8.71GPa) after hot isostatic pressing at 500°C.
4. However, the ductility of these nano-intermetallic dispersed amorphous matrix composites is not satisfactory and failure occurs within elastic limit.

References

[1] Masumoto T. Recent progress in amorphous metallic materials in Japan Mater Sci Eng A 1994; 179/180:8.

[2] Kiminami CS, Basim ND, Kaufman MJ, Amateau MF, Eden TJ, Galbraith GJ. Challenges in the development of aluminum-based bulk amorphous alloys-Key Eng Mater 2001; 189–191:503.

[3] Inoue A. Stabilization of metallic supercooled liquid and bulk amorphous alloys, Acta Mater 2000; 48:279.

[4] Fecht H.J, in: Koch C.C. (Ed.), Nanostructured Materials—Processing, Properties, and Applications, Noyes Publication, William Andrew Publishing, Norwich, NY, USA, 2002, p. 73.

[5] Koch CC. In: Cahn RW, Hassan P, Kramer EJ, editors. Processing of metals and alloys, vol. Weinheim: VCH Publication; 1991. p. 193.

[6] Suryanarayana C. Mechanical alloying and milling, Prog Mater Sci 2001;46:1.

[7] Eckert J, Schultz L. Urban K, Formation of quasicrystals by mechanical alloying, Appl. Phys. Lett. 55 (1989) 117.

[8] El-Eskandarany MS, Aoki K, Suzuki K, Scripta Metall. Mater. 36 (1997) 1001.

[9] Dimitrov H, Blazquez JS, Latuch J, Kulik T. Microstructure and mechanical properties of bulk nanocrystalline $Al_{88}Mm_5Ni_5Fe_2$ alloy consolidated at high pressure, Intermetallics 2007;15: 891-900.

[10] Kawamura Y, Mano H, Inoue A, Nanocrystalline aluminum bulk alloys with a high strength of 1420 MPa produced by the consolidation of amorphous powders, Scripta Mater. 44 (2001) 1599–1604.

[11] Roy D, Kumari S, Mitra R, Manna I, Microstructure and mechanical properties of mechanically alloyed and spark plasma sintered amorphous–nanocrystalline $Al_{65}Cu_{20}Ti_{15}$ intermetallic matrix composite reinforced with TiO_2 nanoparticles, Intermetallics 15 (2007) 1595.

[12] Inoue A, Nakazato K, Kawamura Y, Masumoto T., The effect of Cu addition on the structure and mechanical properties of Al □Ni□M (M □Ce or Nd) amorphous alloys containing nanoscale f.c.c.-Al particles, Mater Sci Eng A 1994; 179-180: 654-8.

[13] Rizzi P, Doglione R, Battezatti L. Mater Sci Eng A 2004; 375-377: 969-74.

[14] Morita T, Mitra R, Weertman JR. Mater Trans Jap Inst Met 2004;45(2):502-8.

[15] RittnerMN, Weertman JR, Eastman JA., Structure—Property Correlations in. Nanocrystalline Al-Zr Alloy Composites, Acta Mater 1996; 44(4):1271-86.

[16] Kumar KS, Van Swygenhoven H, Suresh S, Mechanical behavior of nanocrystalline metals and alloys, Acta Mater 2003; 51:5743-74.

[17] Atkinson HV, Davies S, Fundamental aspects of hot isostatic pressing: An overview, Metall. Mater. Trans. A 31 (2000) 2981–3000.

[18] Gubicza J, Dirras G, Szommer P, Bacroix B, Microstructure and yield strength of ultrafine grained aluminum processed by hot isostatic pressing,, Materials Science and Engineering A 458 (2007) 385–390

[19] Atkinson HV, and Rickinson BA, Hot Isostatic Processing, Adam Hilger, London, 1991

[20] Atkinson HV, Zulfia A, Lima Filho A, Jones H, King S, Hot isostatic processing of metal matrix composites, Materials & Design, Vol. 18, pp. 243-245, 1997

[21] Tjong SC, Tam KF, Mechanical and thermal expansion of hipped Al-TiB2 composites, Materials Chemistry and Physics 97 (2006) 91–97

[22] Hankin GL., Toloczko MB, Hamilton ML, Garner FA, Faulkner RG., Shear punch testing of 59Ni isotopically-doped model austenitic alloys after irradiation in FFTF at different He/dpa ratios, J. Nucl. Mater. 1998, vol. 258-263, pp. 1657-1663

[23] Toloczko MB, Hamilton ML, Lucas GE, Ductility correlations between shear punch and uniaxial tensile test data, J. Nucl. Mater. 2000, vol. 283-287, pp. 987-991

[24] Hankin GL, Toloczko MB, Hamilton ML, Faulkner RG, Validation of the shear punch-tensile correlation technique using irradiated materials, J. Nucl. Mater. 1998, vol. 258-263, pp. 1651-1656

[25] Leo'n CA, Drew RAL., Mater. Lett. 2002, vol. 56, pp. 812-816

[26] Guduru RK, Darling KA, Kishore R, Scattergood RO, Koch CC, Murthy KL, J Mater. Sci. Eng. 2007, vol. 42, pp. 5581-5588

[27] Roy D, Mitra R, Fedyk R, Witczak Z, Lojkowski W, Manna I, Synthesis and characterization of in situ nanocrystalline intermetallic phase reinforced AlTiSi amorphous matrix compositeWitczak Z, Mater. Sci. Eng. A 239 (1997) p.206.

[28] Witczak Z, Mater. Sci. Eng. A 239 (1997) p.206.

[29] Guduru RK, Darling KA., Kishore R, Scattergood RO, Koch CC, Murthy KL, "Evaluation of mechanical properties using shear-punch testing, Mater. Sci. Eng. A 2005, vol. 395, pp. 307-314

[30] Guduru RK, Nagasekhar AV, Scattergood RO, Koch CC, Murthy KL, "Finite element analysis of a shear punch test, Met Trans. 2006, vol. 37, pp. 1477

[31] Nandi P, Chattopadhyay PP, Nambissan PMG, Banhart F, Fecht HJ, Manna I, Microstructural aspects and positron annihilation study on solid state synthesis of amorphous and nanocrystalline $Al_{60-x}Ti_{40}Si_x$alloys prepared by mechanical alloying, J. Non-Cryst. Solids 351 (2005) 2485.

[32] Manna I, Nandi P, Bandyopadhyay B, Ghoshray K, Ghoshray A, Microstructural and nuclear magnetic resonance studies of solid state amorphization in Al-Ti-Si composites, Acta Mater. 52 (2004) 4133.

[33] Palumbo G, Thorpe SJ, Aust KT, On the contribution of triple junctions to the structure and properties of nanocrystalline materials, Scripta Mater. 24 1347 (1990).

[34] Haasz.T. R., Aust. K. T., Palumbo. G., El-Sherik. A. M., Erb. U., Intercrystalline density of nanocrystalline nickel, Scripta Mater., 32 (1995) 423-426

[35] Sergueeva AV, Mara, NA Kuntz JD, Branagan DJ, Mukherjee AK., Shear band formation and ductility of metallic glasses, Mater Sci Eng A 2004, vol. 383, pp. 219-223

[36] Kimura H, Masumoto T: Amorphous metallic alloys. In: Luborsky FE, editor. Butterworth and Co. publishers Ltd.; 1983. p. 201

[37] Guduru RK, Darling KA, Scattergood RO, Koch CC, Murty KL, Bakkal M., Shih A, Shear punch tests for a bulk metallic glass, J. Intermetallics. 2006, vol.14, pp. 1411-1416

[38] Liu CT, Heatherly L, Easton DS, Carmichael CA, Schneibel JH, Chen CH , Test environments and mechanical properties of Zr-base bulk amorphous alloys, Metall Mater Trans A 1998;29:1811.